HNUE JOURNAL OF SCIENCE
Natural Sciences 2024, Volume 69, Issue 1, pp. 40-50
This paper is available online at http://stdb.hnue.edu.vn
DOI: 10.18173/2354-1059.2024-0004

PHYSICAL VAPOR DEPOSITION AND CHEMICAL VAPOR DEPOSITION APPROACHES FOR CONTROLLED GROWTH OF WSe_2 SINGLE-LAYER

Nguyen Anh Duc* and Nguyen Thi Nhan
Faculty of Basic-Fundamental Sciences, Vietnam Maritime University, Hanoi city, Vietnam
*Corresponding author: Nguyen Anh Duc, e-mail: ducna@vimaru.edu.vn

Received February 21, 2024. Revised March 22, 2024. Accepted March 29, 2024.

Abstract. In this paper, two-dimensional ultrathin films of tungsten diselenide (2D-WSe_2) are synthesized on Si/SiO_2 substrate by using two approaches, physical vapor deposition (PVD) and chemical vapor deposition (CVD). The essential parameters of deposition conditions including temperature, pressure, and gas flow of both methods are presented. The samples were examined for their morphology by optical microscopy (OM), scanning electron microscopy (SEM), atomic force microscopy (AFM), and for the crystal lattice vibration properties by Raman scattering spectrum. The results show that the single crystal flakes are located separately in hexagonal or triangular shapes with edge lengths ranging from 20 µm to 100 µm, or can be linked together to form a continuous film. The thickness of most of the film area obtained from both methods can be controlled to a single layer (1L-WSe_2). In addition, the photoluminescence spectra (PL) of the samples were investigated, which indirectly evaluated the crystallization quality of the thin films prepared from the two methods.
Keywords: two-dimensional nanomaterial, single-layer WSe_2, physical vapor deposition, chemical vapor deposition.

1. Introduction

Since the discovery of graphene [1], two-dimensional (2D) materials have gained tremendous attention in the scientific community because of their interesting physical properties along with great potential applications in new-generation electronic and optoelectronic technologies [2]-[5]. Although graphene has been widely researched and is far superior to other 2D materials, it is quite challenging to practically apply graphene to semiconductor and/or optoelectronic devices because it does not possess an energy bandgap [6], [7]. Therefore, 2D materials with large enough bandgaps such as transition metal dichalcogenides (TMDCs) are increasingly attracting interest and expectation [5], [8]. Similar to the layer structure of graphene, TMDC materials, typically MoS_2 and WSe_2, possess atomic-thickness single-layers bonded together by weak van der Waals forces.

Thus, each atomic single-layer of these materials can be easily mechanically separated from the bulk crystals like graphene [1], [9], [10]. For example, Hui Fang et al. obtained 1L-WSe_2 flakes by simply using a sticky tape, the authors also designed a p-type field-sensing transistor (p-FETs) based on such 2D thin layer, and a high performance was achieved with a ratio of $I_{ON}/I_{OFF} > 10^6$ [11]. Overall, this top-down fabrication technique enables the obtaining of 1L-WSe_2 flakes with a perfect crystal structure (defect-free), providing essential information for basic research.

To control the number of material layers uniformly over a large area for research and application, 1L-WSe_2 film deposition techniques using a bottom-up approach have been developed, of which two methods CVD and PVD have been typical [12], [13]. The CVD method with a simple vacuum system enables the fabrication of large-area single-crystal flakes 1L-WSe_2 and does not require too high a working temperature. Compared to the 1L-MoS_2, manufacturing 1L-WSe_2 using CVD is relatively more challenging, because the powder precursor selenium (Se) is less chemically active than sulfur (S), and the precursor WO_3 is more difficult to sublimate than MoO_3. Therefore, there often exists a significant amount of unexpected defects in the material crystal, which in turn leads to many disadvantages for optoelectronic applications, in which the formation and recombination of intrinsic electron-hole pairs in the material is difficult to observe straightforwardly [14]. This drawback may be because the chemical reaction of the precursor (WO_3 and Se) during the crystallization of the WSe_2 film (cooling stage) remains, creating unexpected vacancies. To improve the properties of the film, chemical reaction mechanisms for WSe_2 film growth have been proposed, but have been not clearly defined [15]. Unlike CVD, the film formation process in the PVD method is simply the vapor transport of WSe_2 molecules starting from the pure powder precursor, evaporating from the high-temperature region, following the carrier gas, and depositing on the substrate surface in the lower temperature zone. By utilizing this technique, 2D-WSe_2 was synthesized by Genevieve Clark's group [13], Hailong Zhou [12], and Guolin Hao [16].

Within the limits of our knowledge, there has been no research using a bottom-up approach to manufacture 1L-WSe_2 with the same quality as the top-down mechanical exfoliation technique. Besides, we believe that PVD has great potential to be the optimal technique to reach that aim. In addition, 1L-WSe_2 has still been less studied compared to 1L-MoS_2 or 1L-WS_2. Moreover, it seems that all previous manufacturing research on 2D-WSe_2 only focused on one certain method; it is very rare to research manufacturing 1L-WSe_2 simultaneously using both PVD and CVD techniques, especially with similar equipment configurations. Therefore, a study comparing two typical bottom-up methods (PVD and CVD) will make important contributions to the development of this material [10], [12], [15], [16]. In this report, 1L-WSe_2 membranes are fabricated using PVD and CVD methods. After observing the morphology by microscopic measurements (OM, SEM, AFM), the photoluminescence spectroscopies were collected and compared, thereby evaluating the degree of purity and completeness of the crystal lattice of the obtained material.

2. Content

2.1. Experimental section

2.1.1. Fabrication of 1L-WSe_2 by CVD method

The process of manufacturing 1L-WSe_2 using the CVD method was carried out in a two-heat zones furnace (sketched in Figure 1a) with the following steps. Firstly, the precursor including ~ 0.3 grams of WO_3 powder (Sigma-Aldrich, 99.99%) and ~ 2 grams of Se powder (Sigma-Aldrich, 99.99%) was prepared on 1 cm diameter graphite boats. The boats containing Se and WO_3 were inserted into a 4-inch diameter quartz tube, respectively at the two midpoints of the two heat zones of the furnace (the distance between these two positions was ~ 28 cm). The SiO_2/Si substrate (oxide layer of 300 nm) was placed face down, facing the WO_3 boat position, with a distance of 0.8 cm vertically to the WO_3 powders. In the first step, the temperature in the WO_3 region was increased to 450 ^oC, and simultaneously in the Se region was increased to 200 ^oC and maintained for 5 minutes. In the next step, the high-temperature zone (WO_3 position) was heated to 920 ^oC, and the Se powder was heated to 450 ^oC with a heating rate of 12 ^oC/min. This reaction condition was kept stable for 15 minutes and then finished by natural cooling to room temperature. The thermal diagram for the entire deposition process is illustrated in Figure 1b. During the entire time, from the initial heating step to cooling to room temperature, a carrier gas of a mixture of ~15 sccm (N_2 + H_2) was continuously introduced into the furnace, whereas the pressure for the film reaction stage ranged from 500 to 600 torr.

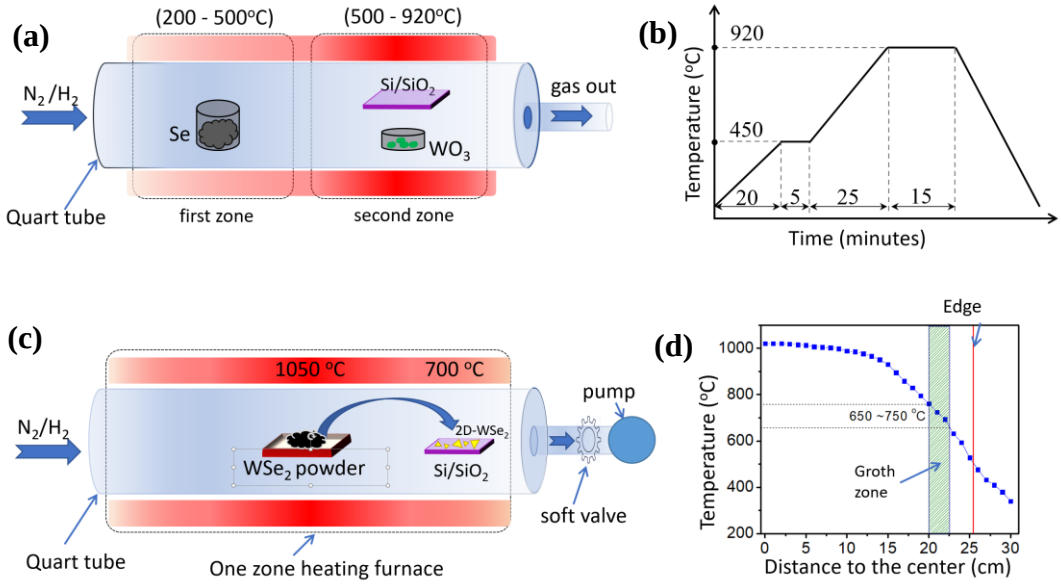

Figure 1. (a, b) Two-heat zones CVD system configuration to the growth of the 1L-WSe_2 and temperature diagram at the center of the second zone where the film formed; (c, d) PVD system configuration diagram using a single-heat zone furnace to deposit 1L-WSe_2 and the dependence of temperature on the distance to the furnace center

2.1.2. Fabrication of 1L-WSe_2 by PVD method

For the fabrication of 2D-WSe_2 using the PVD method, we performed it in a furnace with one thermal zone, illustrated in Figure 1c. The experiment was started by introducing approximately 0.5 grams of pure WSe_2 powder precursor (Sigma-Aldrich, 99.99%) to the center of a quartz tube (4-inch diameter - the same size as the quartz tube used in the CVD method), corresponding to the midpoint of the furnace. The SiO_2/Si substrate was placed near the edge of the furnace, towards the exiting gas flow. At the center of the furnace, the temperature was increased from room temperature to 1050 ^oC in 50 minutes to evaporate the WSe_2 raw powder. Figure 1d demonstrates the thermal gradient in the growth chamber when the center temperature reaches 1050 ^oC, where the *x*-axis is the distance from the center to the edge of the chamber. The corresponding temperature at the deposition zone is in the range of 650 - 750 ^oC. The operating pressure in the chamber was adjusted by a soft valve to approximately 200 mTorr to obtain the largest size of a single crystal atomic-thickness film.

2.1.3. Characterization

The morphology of 1L-WSe_2 sheets was first observed by an optical microscope (OM), and a scanning electron microscope (Scanning electron microscopy - SEM, JEOL code JSM-6500F). The thickness of the material was determined by atomic force microscopy (AFM, equipment code MFP - 3D Origin). The lattice vibration properties were evaluated by Raman scattering spectrum, with device labels Dongwoo Optron, Ramboss-Star, and an excitation laser beam with wavelength λ = 473 nm. Optical properties were studied by photoluminescence emission spectroscopy (PL) at room temperature.

2.2. Results and discussion

2.2.1. Morphology of 1L-WSe_2

First of all, the morphology of the material can be easily observed by using an optical microscope, Figures 2a-f are photographs of typical 2D-WSe_2 flakes fabricated by CVD. When the grown temperature was lower than 900 ^oC (Figure 2a-b) or high up to 1000 ^oC (Figure 2c), the majority of CVD_WSe_2 flakes were multilayer (bright cyan color area). As explained by Bilu Liu et al. [15], low temperatures cause a lack of mobile active reactants, thereby causing the film to tend to grow into a 3D structure; while a too-high temperature leads to a too-high reactant density, which also causes the film to thicken. At a temperature of 920 ^oC, the 2D-WSe_2 film appears mostly single-layer (Figure 2d-f). The as-grown 1L-WSe_2 films appear in hexagonal or triangular shapes, which are particularly due to the hexagonal structure of its lattice crystal [17], consistent with previous reports [15], [18].

In most previous papers, a mixture of Ar and H_2 was used as the component of the carrier gas to grow 2D-WSe_2, in which the ratio (Ar: H_2) was (16:1) in Ref. [15], (9:1) in [18], and (4:1) in [19] as examples. In this study, we used N_2 gas instead of Ar. We found that, when the carrier gas flow ratio (N_2:H_2) was (5:1), the sample contained many 2D-WSe_2 sheets in hexagonal shape (Figures 2d-e); when the ratio (N_2:H_2) was (3:1), it typically appeared in the form of a triangle (Figure 2f). In general, hexagonal flakes have an average diameter of ~ 150 µm, significantly larger than triangular flakes (average size ~ 40 µm).

The material film located in the middle of the SiO_2 substrate formed a continuous membrane on the left side of Figure 2d, which was due to its closer distance to the WO_3 raw material. In fact, among experiments, although much effort has been made to precisely maintain the fabrication conditions, certain samples appeared to have significantly thicker areas (the white edge area in Figure 2d). This is because the environment of the growth chamber changes uncontrollably among experiments, and is extremely sensitive in affecting the formation of the 2D films. Moreover, although the triangular flakes were smaller in breadth, the edges were exceedingly sharp, and sharper than the edges of the hexagonal plates, suggesting that the triangular flakes were better crystallized and more evenly distributed.

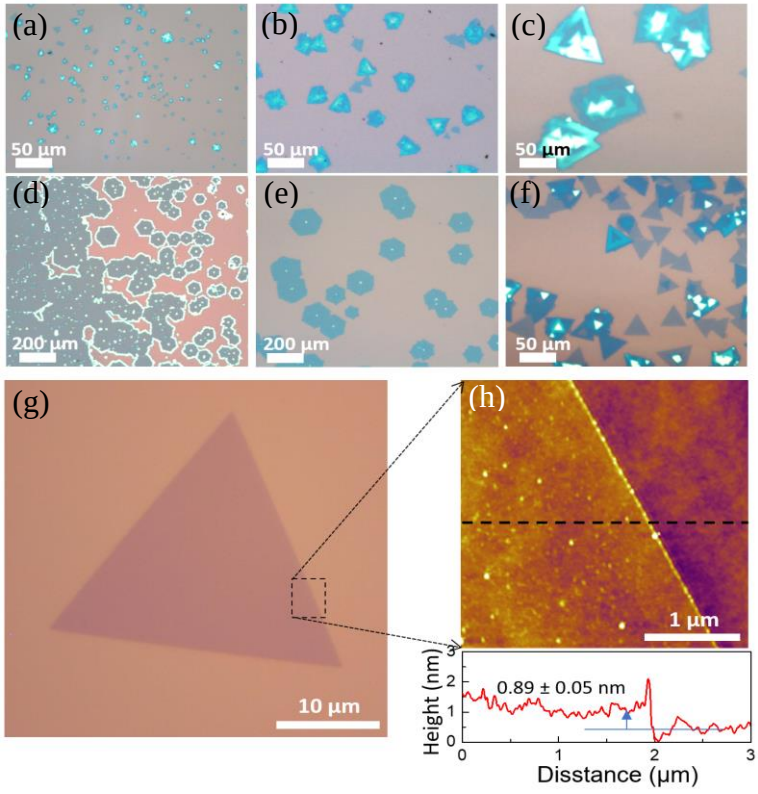

Figure 2. The morphology of 1L-WSe_2 was obtained by the CVD method. OM images of multilayers CVD_WSe_2 samples were obtained at (a) 800 °C, (b) 850 °C, (c) 1000 °C. (d-f) OM images of CVD_1L-WSe_2 grown at 920 °C and the carrier gas flow ratio N_2:H_2 of 5:1, and (f-g) that of (3:1). (h) AFM images of a typical triangular CVD_1L-WSe_2 flake

Next, the surface morphology as well as the thickness of a typical triangular flake (Figure 2g) was further investigated using an atomic force microscope, the results are presented in Figure 2h. The image determined that the film surface was relatively uniform, with an average thickness of 0.89 nm, which is the typical thickness of a single layer, including a layer of W atoms sandwiched between two layers of Se atoms [12], [15]. Generally, by using the shown CVD system configuration, operating with the presented parameters and the carrier gas ratio (N_2:H_2) of (3:1), we have obtained the optimum quality of 1L-WSe_2 films.

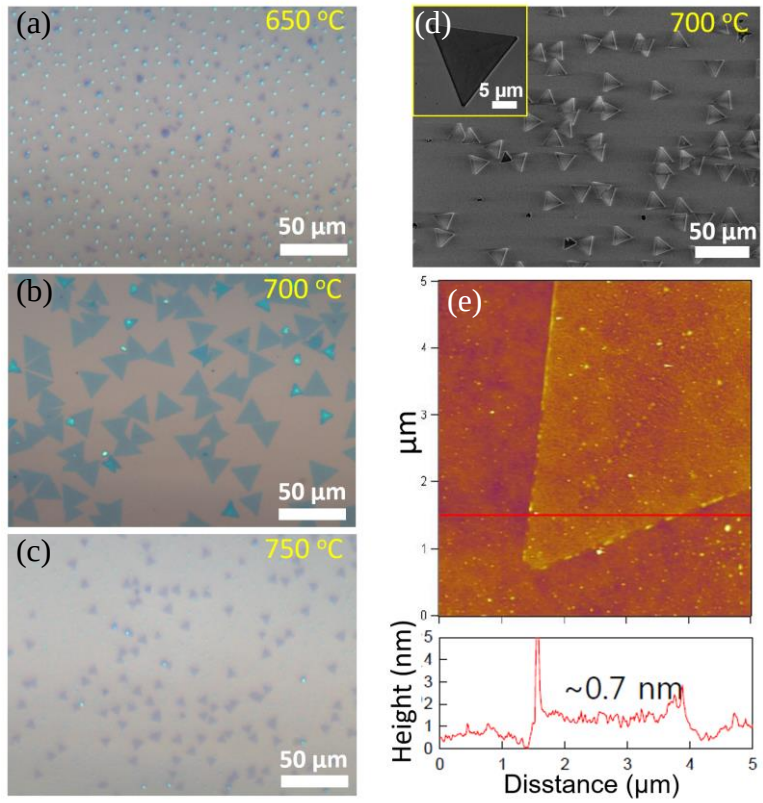

Figure 3. The morphology of 1L-WSe_2 material prepared by PVD method. (a-c) Optical microscope images of PVD_1L-WSe_2 samples at temperatures 650, 700, and 750 °C. (d-e) SEM and AFM images of the 700 °C sample respectively

For the 2D-WSe_2 membrane fabricated by the PVD method, the parameters of growth conditions that need to be cautiously controlled include deposition temperature, carrier gas flow, and growth pressure. The buffer valve of the growth system also plays a crucial role, enabling the adjustment of the working pressure to match the amount of introduced carrier gases. Q. Feng et al. have published a procedure for growing 2D-TMDC materials using the PVD method with the following steps: absorption/release, diffusion, and reaction, in which the nucleation and saturation processes are controlled by the temperature gradient in the growth chamber. In this report, we controlled the saturation process by adjusting the pressure through a buffer valve. If there were many seeds, the size of the WSe_2 sheets was smaller, and the rate of multilayer film formation was also higher. The optimal growth pressure for the PVD system we implemented was 170 Torr, corresponding to a carrier gas flow of 15 sccm N_2 and 0.8 sccm H_2.

Figure 3a-c reveals optical microscope images of typical PVD-WSe_2 flakes, respectively at substrate positions with temperatures varying from 650 - 750 °C. We found that, at a lower temperature, although the nucleation step takes place more easily, it is difficult to attain a large area of single-layer films, while at a higher temperature, saturation, and nucleation seem scarce, which also leads to smaller flakes. Particularly, the 650 °C samples appeared to have a high density of small and thick particles (brighter colored round dots). At the same time, the high-temperature sample (750 °C) appeared to have

sparsely located single-layer particles (triangles) but the size was also small (~ 5 µm). At the position of 700 °C, we achieved the most optimal film, in which most of the triangular single-layer flakes exhibited sharp edges and larger sizes. Then, the 700 °C sample was selected to further investigate the scanning electron microscope (SEM image in Figure 3d) and atomic force microscope (AFM) (Figure 3e). The results demonstrated that the films were single-layer (thickness < 1 nm) and the width of the single crystal flake reached ~ 20 µm.

2.2.2. Vibration properties of the crystal lattice of the 1L-WSe_2

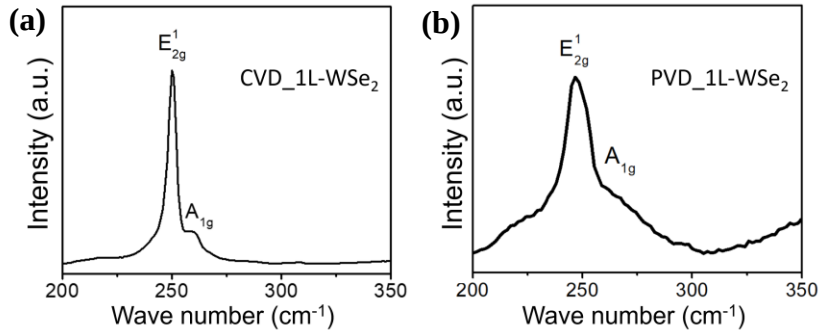

Figure 4. (a) and (b) Raman scattering spectrum of 1L-WSe_2 by CVD and PVD

Figure 4a-b presents the Raman scattering spectra of 1L-WSe_2 samples. The two typical peaks observed in both samples appeared at wavenumber positions of 247 cm^{-1} and 259 cm^{-1}, respectively, corresponding to the active Raman modes E^1_{2g} and A^1_g of 1L-WSe_2 in the 2H hexagonal structure, in which the E^1_{2g} vibration mode is horizontal (oriented in the direction of the membrane surface), and A^1_g vibration mode is vertical (in the direction perpendicular to the membrane surface) [20]. It is well known that 1L-WSe_2 has a crystal structure and chemical formula essentially similar to 1L-MoS_2. For 1L-MoS_2, we can easily distinguish the two Raman peaks mentioned above because their intensity is approximately the same and the distance is large, and the distance between the two peaks can indicate the thickness of the crystal sheet [20], [21]. However, these two peaks in 1L-WSe_2 are located close to each other and the intensity of the A^1_g peak is significantly smaller than that of E^1_{2g}, and frequently appears unclearly, hidden in the shoulder of the E^1_{2g} peak; it is not easy to rely on the spectrum Raman scattering to confirm the number of layers as well as to assess the level of the lattice perfection of the membrane. To compare the level of perfection of the 1L-WSe_2 crystal structure produced by the two methods, we can rely on the luminescent features of the material.

2.2.3. Luminescent properties of 1L-WSe_2

Figure 5a presents the room temperature photoluminescence (PL) emission spectrum of 1L-WSe_2 grown by PVD and CVD, compared with that of the bulk type (precursor powder). Similar to MoS_2, we can easily ascertain whether the WSe_2 film is single-layer or multi-layer by observing the PL spectrum. The quenching of the photoluminescence emission of the bulk TMDC materials is due to the alter in energy band structure compared to the monolayer, in which the bottom of the conduction band in wave vector space strongly shifts away from the position of the top of the valence band as the number of layers increases. Literature has shown that 1L-WSe_2 has an energy bandgap of ~ 2.58 eV [22], on the other hand, the electron-hole pairs in 1L-WSe_2 have large binding energy

(~ 0.9 eV) [23]. Therefore, the radiative recombination energy of most of the electron-hole pairs (A-excitons or free excitons) of 1L-WSe_2 was predicted to be approximately 1.68 eV, equivalent to a wavelength of ~ 740 nm [22]. Thus, the appearance of a strong emission peak at a wavelength of 742 nm of PVD_1L-WSe_2 in Figure 5a (blue line) is consistent with published data. This result reflects that the 1L-WSe_2 sample synthesized by the PVP technique has good crystallization quality. In a sense, this result is beneficial for optoelectronic applications, where the mostly impurity-free 1L-WSe_2 film enables the observation of optically active/inactive excitons, so-called bright/dark excitons [24]. Particularly, the lifetime of dark excitons is typically two orders of magnitude longer than that of their bright counterparts, which has significant benefits for quantum computing science and/or investigation of Bose-Einstein condensation [25].

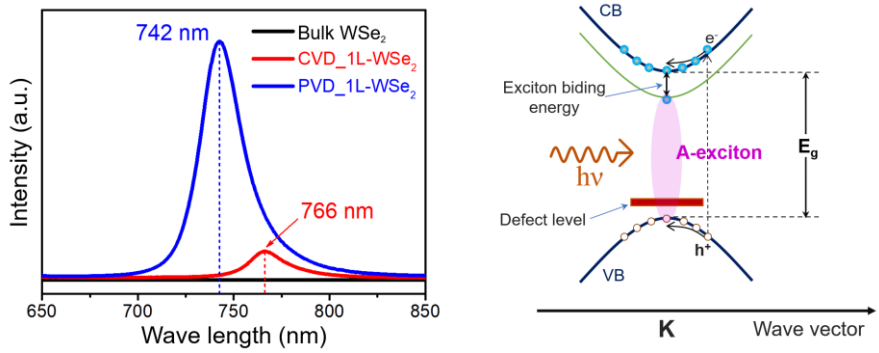

Figure 5. (a) Photoluminescence spectrum of 1L-WSe_2 (film) prepared by two methods (CVD and PVD) and bulk WSe_2 (powder); (b) Energy band diagram describing the excitonic emission recombination in the wave vector space of 1L-WSe_2

For the sample fabricated by CVD, as can be seen in Figure 5a (red line), the PL peak position is located at a wavelength of 766 nm (~ 1.62 eV), which is well in agreement with the literature, such as 766 nm [12], 1.61 eV [15], and 1.60 eV [18]. However, the as-seen PL spectrum of CVD_1L-WSe_2 exhibited a distinct change in comparison with that of PVD_1L-WSe_2, in which the emission intensity was significantly reduced (~ 10 times, with the same excitation conditions), and the peak position shifted quite strongly toward the larger wavelength direction (~ 24 nm from the position of the PVD one). The plausible reason can be the considerable presence of defect sites in the CVD_WSe_2 sample, thereby forming defect states in the energy bandgap as illustrated in Figure 5b. According to Shuai Zhang et al. [14], the vacancies of the tungsten atom (W) in the structure of 1L-WSe_2 form local excitonic states with recombination energies close to the value of the free A-exciton, this may be the essential reason for the strong shift of the PL emission peak in the CVD_1L-WSe_2 sample. It is also worth noting here that, these defects of *W*-vacancies are likely the origin of *p* doping in 1L-WSe_2, which presents a natural way to create a *p-n* junction using a 2D heterostructure [14].

3. Conclusions

In summary, we have successfully fabricated and investigated the basic properties of the two-dimensional WSe_2 semiconductor material using two approaches PVD and CVD. As evidenced by microscopic observation results, the single crystal flakes of the samples

showed a hexagonal or triangular shape with widths of a few dozen to more than a hundred micrometers and a thickness of only a single atomic layer. The optimal conditions in the CVD method for the substrate surface to contain mostly large-area, well-crystallized 1L-WSe_2 single crystal flake include temperature ~ 920 ^oC, pressure ~ 550 Torr, and a carrier gas ratio (N_2:H_2) of (3:1). For the PVD method with a deposition chamber (quartz tube) of similar size, the raw-material evaporation temperature ~ 1050 ^oC, pressure ~ 200 mTorr, and substrate temperature ~ 700 ^oC are the parameters that should be established to obtain a high-quality film. In general, CVD_1L-WSe_2 single crystal flakes reveal a larger area but contain the lattice structure containing more defect sites than PVD_1L-WSe_2.

REFERENCES

[1] Novoselov KS, Geim AK, Morozov SV, Jiang D, Zhang Y, Dubonos SV, Grigorieva IV & Firsov AA, (2004). Electric Field Effect in Atomically Thin Carbon Films. *Science,* 306(5696), 666-669. DOI: 10.1126/science.110289.

[2] Kumbhakar P, Jayan JS, Sreedevi Madhavikutty A, Sreeram PR, Saritha A, Ito T & Tiwary CS, (2023). Prospective applications of two-dimensional materials beyond laboratory frontiers: A review. *iScience,* 26(5), 106671. DOI: 10.1016/j.isci.2023. 106671.

[3] Shanmugam V, Mensah RA, Babu K, Gawusu S, Chanda A, Tu Y, Neisiany RE, Försth M, Sas G & Das O, (2022). A Review of the Synthesis, Properties, and Applications of 2D Materials. *Particle & Particle Systems Characterization,* 39(6), 2200031. DOI: 10.1002/ppsc.202200031.

[4] Naikoo GA, Arshad F, Almas M, Hassan IU, Pedram MZ, Aljabali AAA, Mishra V, Serrano-Aroca A, Birkett M, Charbe NB, Goyal R, Negi P, El-Tanani M & Tambuwala MM, (2022). 2D materials, synthesis, characterization, and toxicity: A critical review. *Chemico-Biological Interactions,* 365(25), 110081. DOI: 10.1016/j.cbi.2022.110081.

[5] Chowdhury T, Sadler EC & Kempa TJ, (2020). Progress and Prospects in Transition-Metal Dichalcogenide Research Beyond 2D. *Chemical Reviews,* 120(22), 12563-12591. DOI: 10.1021/acs.chemrev.0c00505.

[6] Lee H, Paeng K & Kim IS, (2018). A review of doping modulation in graphene. *Synthetic Metals,* 244, 36-47. DOI: 10.1016/j.synthmet.2018.07.001.

[7] Nguyen HY, Le XH, Pham NT, Phan NH & Pham TN, (2020). Synthesis of graphene quantum dots and Nitrogen-doped graphene quantum dots: Raman characterization and their optical properties. *HNUE Journal of Science: Natural Science,* 65(3), 82-90. DOI: 10.18173/2354-1059.2020-0010

[8] Joseph S, Mohan J, Lakshmy S, Thomas S, Chakraborty B, Thomas S & Kalarikkal N, (2023). A review of the synthesis, properties, and applications of 2D transition metal dichalcogenides and their heterostructures. *Materials Chemistry and Physics,* 297(1), 127332. DOI: 10.1016/j.matchemphys.2023.127332.

[9] Li Y, Kuang G, Jiao Z, Yao L & Duan R, (2022). Recent progress on the mechanical exfoliation of 2D transition metal dichalcogenides. *Materials Research Express*, 9(12), 122001. DOI: 10.1088/2053-1591/aca6c6.

[10] Li H, Wu J, Yin Z & Zhang H, (2014). Preparation and applications of mechanically exfoliated single-layer and multilayer MoS_2 and WSe_2 nanosheets. *Acc. Chemical Research*, 47(4), 1067-75. DOI: 10.1021/ar4002312.

[11] Fang H, Chuang S, Chang TC, Takei K, Takahashi T & Javey A, (2012). High-Performance Single Layered WSe2 p-FETs with Chemically Doped Contacts. *Nano Letters*, 12(7), 3788-3792. DOI: 10.1021/nl301702r.

[12] Zhou H, Wang C, Shaw JC, Cheng R, Chen Y, Huang X, Liu Y, Weiss NO, Lin Z, Huang Y & Duan X, (2015). Large area growth and electrical properties of p-type WSe_2 atomic layers. *Nano Letters*, 15(1), 709-13. DOI: 10.1021/nl504256y.

[13] Clark G, Wu S, Rivera P, Finney J, Nguyen P, Cobden DH & Xu X, (2014). Vapor-transport growth of high optical quality WSe_2 monolayers. *APL Materials*, 2(10), 101101. DOI: 10.1063/1.4896591.

[14] Zhang S, Wang C-G, Li M-Y, Huang D, Li L-J, Ji W & Wu S, (2017). Defect Structure of Localized Excitons in a WSe_2 Monolayer. *Physical Review Letters*, 119(4), 161302 (1-d). DOI: 10.1103/PhysRevLett.119.046101.

[15] Liu B, Fathi M, Chen L, Abbas A, Ma Y & Zhou C, (2015). Chemical Vapor Deposition Growth of Monolayer WSe_2 with Tunable Device Characteristics and Growth Mechanism Study. *ACS Nano*, 9(6), 6119-6127. DOI: 10.1021/acsnano.5b01301.

[16] Hao G, Kou L, Lu D, Peng J, Li J, Tang C & Zhong J, (2016). Electrostatic properties of two-dimensional WSe_2 nanostructures. *Journal of Applied Physics*, 119(3), 035301. DOI: 10.1063/1.4940160.

[17] Cheng Q, Pang J, Sun D, Wang J, Zhang S, Liu F, Chen Y, Yang R, Liang N, Lu X, Ji Y, Wang J, Zhang C, Sang Y, Liu H & Zhou W, (2020). WSe_2 2D p-type semiconductor-based electronic devices for information technology: Design, preparation, and applications. *InfoMat*, 2(4), 656-697. DOI: 10.1002/inf2.12093.

[18] Wang X, Li Y, Zhuo L, Zheng J, Peng X, Jiao Z, Xiong X, Han J & Xiao W, (2018). Controllable growth of two-dimensional WSe_2 using salt as co-solvent. *CrystEngComm*, 20(40), 6267-6272. DOI: 10.1039/C8CE01162A.

[19] Huang J-K, Pu J, Hsu C-L, Chiu M-H, Juang Z-Y, Chang Y-H, Chang W-H, Iwasa Y, Takenobu T & Li L-J, (2014). Large-Area Synthesis of Highly Crystalline WSe_2 Monolayers and Device Applications. *ACS Nano*, 8(1), 923-930. DOI: 10.1021/nn405719x.

[20] Tonndorf P, Schmidt R, Böttger P, Zhang X, Börner J, Liebig A, Albrecht M, Kloc C, Gordan O, Zahn DRT, Michaelis de Vasconcellos S & Bratschitsch R, (2013). Photoluminescence emission and Raman response of monolayer MoS_2, $MoSe_2$, and WSe_2. *Optics Express*, 21(4), 4908-4916. DOI: 10.1364/OE.21.004908.

[21] Lee C, Yan H, Brus LE, Heinz TF, Hone J & Ryu S, (2010). Anomalous Lattice Vibrations of Single- and Few-Layer MoS_2. *ACS Nano*, 4(5), 2695-2700. DOI: 10.1021/nn1003937.

[22] Yan T, Qiao X, Liu X, Tan P & Zhang X, (2014). Photoluminescence properties and exciton dynamics in monolayer WSe_2. *Applied Physics Letters,* 105(10), 101901 (1-4). DOI: 10.1063/1.4895471.

[23] Ramasubramaniam A, (2012). Large excitonic effects in monolayers of molybdenum and tungsten dichalcogenides. *Physical Review B,* 86(11), 115409 (1-6). DOI: 10.1103/PhysRevB.86.115409.

[24] Malic E, Selig M, Feierabend M, Brem S, Christiansen D, Wendler F, Knorr A & Berghäuser G, (2018). Dark excitons in transition metal dichalcogenides. *Physical Review Materials,* 2(1), 014002-1-014002-7. DOI: 10.1103/PhysRevMaterials. 2.014002.

[25] Robert C, Amand T, Cadiz F, Lagarde D, Courtade E, Manca M, Taniguchi T, Watanabe K, Urbaszek B & Marie X, (2017). Fine structure and lifetime of dark excitons in transition metal dichalcogenide monolayers. *Physical Review B,* 96(15), 155423. DOI: 10.1103/PhysRevB.96.155423.